Journal of Inorganic and General Chemistry
ZAAC
Zeitschrift für anorganische und allgemeine Chemie
DOI: 10.1002/zaac.201900356
ARTICLE

Electrochemical CO_2 and Proton Reduction by a Co(dithiacyclam) Complex

Linda Iffland,[a] Daniel Siegmund,[b] and Ulf-Peter Apfel*[a,b]

Dedicated to Manfred Scheer on the Occasion of his 65th Birthday

Abstract. While $[Ni(cyclam)]^{2+}$ and $[Ni(dithiacyclam)]^{2+}$ complexes were shown to be potent electrocatalysts for the CO_2 conversion, their respective Co complexes hitherto received only little attention. Herein, we report on the Co^{II} complexes of the cyclam and dithiacyclam platform, describe their synthesis and reveal their rich solvent dependent coordination chemistry. We show that sulfur implementation into the cyclam moiety leads to a switch from a low spin Co^{II} complex in $[Co(cyclam)]^{2+}$ to a high spin form in $[Co(dithiacyclam)]^{2+}$. Notably, while both complexes are capable to perform the reduction of CO_2 to CO, H_2 formation is generally preferred. Along this line, the complexes were shown to enable proton reduction from acetic acid. However, in comparison to $[Co(cyclam)]^{2+}$, the altered electronics make $[Co(dithiacyclam)]^{2+}$ complexes prone to deposit on the glassy carbon working electrode over time leading to an overall low faradaic efficiency for the reduction of protons or CO_2.

Introduction

In order to replace fossil fuels as an energy source as well as a raw material for the chemical industry, intensive research is currently undertaken.[1–5] With its high energy density per kilogram,[6,7] hydrogen is an attractive energy storage molecule and can be obtained by water splitting. However, its low energy density per volume likewise pushes the need for alternative energy storage systems. Herein, carbon dioxide represents a potential alternative to conventional used carbon sources, like fossil fuels and enables the efficient storage of energy. For an efficient hydrogen generation and the conversion of CO_2, suitable catalysts are required.[1,8,9]

In contrast to the industrially used heterogeneous catalysts, the manifold spectroscopic techniques available in homogeneous catalysis enable scientists to reveal relations between structural features, their catalytic performance and the underlying mechanistic details.[10–12] Such homogeneous catalysts are often transition metal-based coordination compounds with versatile ligand frameworks.[9,12] Notably, natural enzymes that perform the activation and conversion of protons and CO_2, commonly utilize 3d metals such as Fe and Ni in their active centers underlining the potential of the 3d metals.[13–17]

Although cobalt has a negligible role in the enzymatic conversion of CO_2 and protons, cobalt complexes are widely used in synthetic approaches as CO_2 reduction or hydrogen evolution catalysts.[12] These complexes commonly feature a metal center with a Co^{II} or Co^{III} resting state coordinated by a macrocyclic chelating ligand.[12] Based on the ligand platform, complexes can be divided into different classes and porphyrin-based compounds[18–20] or cobaloximes[21–24] are among the most active catalyst platforms.

The macrocyclic aza-ligand cyclam **L1**, a 14-membered ring system with four nitrogen donor atoms (Scheme 1) is another promising ligand platform for CO_2 and proton conversion processes.[25,26] Notably, one of the most prominent homogeneous transition-metal catalyst for electrochemical CO_2 reduction is $[Ni(cyclam)]^{2+}$.[27–30] Therefore, it is astonishing that up to now only little is known about the corresponding Co complex and a majority of reports focuses on the cyclam-like diimine ligands **L2** and **L3** (Scheme 1).[25,31] The corresponding Co complexes were already investigated for their catalytic activity in the electrochemical reduction of CO_2 in 1980 by *Fisher* and *Eisenberg*.[25] Under CO_2 atmosphere in water/acetonitrile (2 : 1), controlled potential coulometry at –1.6 V (Co^{II}**L2**) and –1.5 V (Co^{II}**L3**) vs. SCE utilizing a mercury working electrode afforded CO and H_2 in a 1 : 1 ratio showing current efficienc-

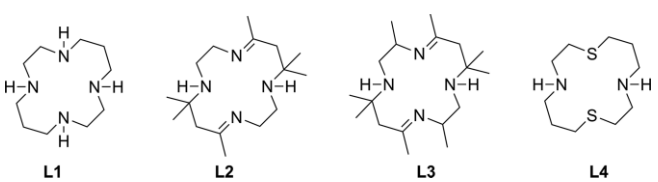

Scheme 1. Macrocylic cyclam derived ligands **L1**–**L4** as ligand platforms for electrocatalytic CO_2 and proton reduction.

* Prof. Dr. U.-P. Apfel
E-Mail: ulf.apfel@rub.de
[a] Inorganic Chemistry I
Ruhr-Universität Bochum
Universitätsstraße 150
44801 Bochum, Germany
[b] Department of Electrosynthesis
Fraunhofer UMSICHT
Osterfelder Straße 3
46047 Oberhausen, Germany
Supporting information for this article is available on the WWW under **http://dx.doi.org/10.1002/zaac.201900356** or from the author.

ies of > 90 %. It is worth mentioning that the extension of the electrolysis from 1.1 h to 19 h resulted in a higher amount of generated H_2 with a product ratio of 1 : 3.6 for CO : H_2. In addition, *Tinnemans* et al. reported the CO_2 reduction by Co^{II}**L2** in pure water affording a CO : H_2 ratio of 1 : 1.6 with decreased overall faradaic efficiency of 62 %.[31]

Notably, with decreasing water content in the electrolyte, the competitive hydrogen generation is suppressed, shifting the product ratio to 2.8 : 1 in favor of CO formation but concomitant with a loss in current efficiency (20 %).[31] At the same time Co^{II}**L2** was investigated as an electron-transfer agent for the photochemical reduction of CO_2.[31] Although CO was detected as reduction product utilizing $[Ru(bipy)_3]^{2+}$ as photosensitizer in ascorbate buffer, H_2 evolution was observed with threefold higher amounts and shows that proton reduction is preferred over CO_2 reduction.

Later on, *Yanagida* et al. reinvestigated the Co^{III} complexes of **L1**, **L2**, and **L3** for the photochemical CO_2 reduction.[32,33] In contrast to earlier studies they replaced the noble-metal photosensitizer by the organic dye *p*-terphenyl, a strong reducing agent (E_{ox} = –2.45 V vs. SCE), and utilized triethylamine as sacrificial electron donor. For Co^{III}**L1** in methanol containing acetonitrile solutions, CO and formate were observed as the main reduction products in a ratio of 2 : 1 and only small amounts of hydrogen were formed. Utilizing dimethylformamide instead of acetonitrile completely prevented the generation of formate. The Co^{III} complexes of **L2** and **L3** exhibited significantly lowered catalytic activity as compared to Co^{III}**L1**.[33] The mechanism and kinetics of the photocatalytical CO_2 reduction system with *p*-terphenyl as photosensitizer were then intensively studied by transient spectroscopy in continuous and flash photolysis experiments.[34] These results showed that $[Co^{I}(\mathbf{L})]^+$ is the catalytic active species and confirmed the existence of the $[Co^{I}(\mathbf{L})(CO_2)]^+$ and $[SCo^{III}(\mathbf{L})(CO_2^{2-})]^+$ (S = solvent) reaction intermediates. The choice of the applied photosensitizer significantly affects the product formation of the photochemical CO_2 reduction due to a solvent-altered reaction mechanism. Using a weaker reduction agent, e.g. phenazine (E_{ox} = –1.2 V vs. SCE), instead of *p*-terphenyl for photocatalytic CO_2 reduction resulted in the preferential formate production.[35,36] Herein, CO and H_2 were observed only in trace amounts. Due to the weaker oxidation potential of the phenazine, it is not possible to form the Co^{I} intermediate required for the CO formation. Instead, a $[Co^{II}(\mathbf{L})(H)]^{2+}$ intermediate is generated and is responsible for the formate production. Electrochemical studies on the CO_2 reduction by a Co^{III} complex bearing **L1** as ligand were hitherto only reported in ionic liquids.[37] Although Co^{III}(**L1**) is able to serve as catalyst precursor and reduces CO_2 to CO, the comparable Ni^{II}(**L1**) complex reveals a ten times higher turnover number as well as a significantly better overall performance.[37]

Inspired by the sulfur-rich coordination environment of the active centers of CO dehydrogenases and hydrogenases, incorporation of sulfur into the macrocyclic cyclam platform revealed Ni^{II}(**L4**) (**L4** = dithiacyclam, 1,8-dithia-4,11-diazacyclotetradecane) and enabled a facilitated CO_2 reduction at more positive potentials and an enhanced H_2 evolution capability relative to Ni^{II}(**L1**).[38] Based on the insufficient electrochemical investigations of the Co^{II}(cyclam) system and our latest results comparing the electrocatalytic activity of Ni^{II} complexes comprising **L1** and **L4**, we became interested in a directed approach to obtain Co^{II}(**L1**) and the hitherto unknown Co^{II} complex of **L4**. We herein report on the catalytic activity of both Co^{II} complexes for electrochemical CO_2 reduction as well as H_2 generation.

Results and Discussion

Complex Synthesis and Properties

Since Co^{II}(**L1**) had already been reported as an air-sensitive compound,[39] reaction of **L1** with $Co(ClO_4)_2{\cdot}6H_2O$ or $[Co(CH_3CN)](ClO_4)_2$ as Co^{II} salts were performed in acetonitrile under the exclusion of air affording **C1** as an orange crystalline material. The successful complexation was supported by electrospray-ionization mass spectrometry (ESI-MS) revealing the characteristic mass peaks at *m*/*z* = 258.1 and 357.9 for the $[Co(\mathbf{L1}\text{-}H)]^+$ and $[Co(\mathbf{L1})(ClO_4)]^+$ fragments. Crystals of **C1** were obtained from methanol solutions and further supported the molecular structure of **C1** showing the expected $[Co(\mathbf{L1})(ClO_4)_2]$ composition (Figure 1) that was already reported in the late 1970s.[39] Compared to the IR spectrum of the as synthesized material and the crystalline material obtained from methanol solutions, IR spectra from $[Co(\mathbf{L1})(ClO_4)_2]$ as synthesized material contained additional signals at 2263 and 2296 cm^{-1} (Figure S1, Supporting Information). These signals remained even after prolongated drying under vacuum and can be assigned to C≡N stretching vibrations in-

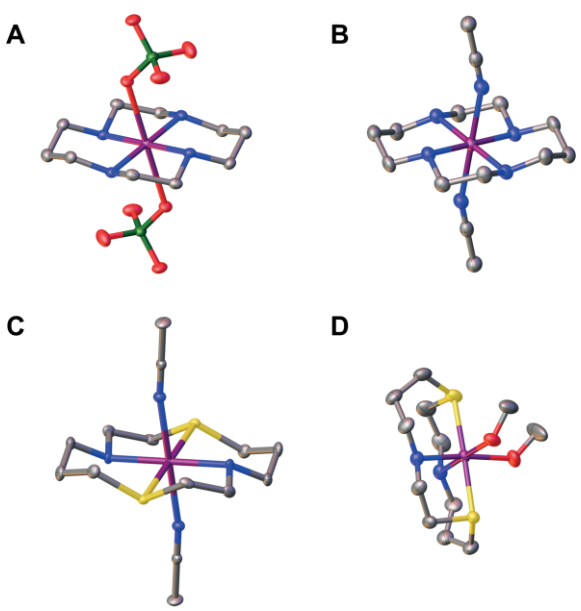

Figure 1. Molecular structure of **C1** obtained by crystallization from (A) methanol and (B) acetonitrile as well as molecular structure of **C2** (C) and **C2′** (D) shown with thermal ellipsoid drawn at the 50 % probability level. Hydrogen atoms and perchlorate counterions for B, C and D are omitted for clarity. Gray: carbon, blue: nitrogen, yellow: sulfur, red: oxygen, green: chlorine, purple: cobalt.

dicating an additional coordination of acetonitrile. A similar solvent-dependent coordination behavior was already reported for Ni^{II}-cyclam derivatives.[40] This assumption was likewise supported by the molecular structure of **C1** obtained from single crystals of a saturated acetonitrile solution (Figure 1). Herein, additional binding of two acetonitrile molecules in the axial positions complete the octahedral coordination sphere of the central metal ion. As seen from averaged Co–N_{L1} distances of 1.99 Å (perchlorate derivative) and 2.00 Å (acetonitrile derivative), the exchange of the axial ligands had no significant effect on the coordination sphere of the central Co^{II} ion.

Similar to the complexation of **L1**, **L4** was treated with one equivalent of $Co(ClO_4)_2{\cdot}6H_2O$ or $[Co(CH_3CN)_6](ClO_4)_2$ in acetonitrile. The formed solid was then recrystallized from acetonitrile by addition of diethyl ether. The formation of the expected Co^{II} complex was confirmed by ESI-MS revealing mass peaks at m/z = 292.0 and 391.9 for the $[Co(\mathbf{L4}\text{-H})]^+$ and $[Co(\mathbf{L4})(ClO_4)]^+$ fragments. The IR spectrum of the obtained crystalline material showed, comparably to **C1**, C≡N stretching bands at 2261 and 2295 cm^{-1} and likewise suggested acetonitrile coordination (Figure S2, Supporting Information). The molecular structure of **C2** further supported this behavior and revealed that nitrogen and sulfur atoms of **L4** occupy the equatorial positions with averaged Co–N_{L4} and Co–S_{L4} distances of 2.02 and 2.24 Å (Figure 1). Comparably to **C1**, two acetonitrile molecules complete the octahedral coordination sphere with averaged Co–N_{CH3CN} distances of 2.24 Å. However, solvent exchange from acetonitrile to methanol leads to a significantly altered molecular structure of **C2**. While the Co^{II} ion still reveals an octahedral coordination sphere, the solvent molecules, methanol, together with the nitrogen atoms of **L4** now occupy the equatorial positions with averaged Co–O and Co–N_{L4} distances of 2.15, respectively 2.11 Å. Thus the sulfur atoms of **L4** occupy the axial positions with averaged Co–S_{L4} distances of 2.47 Å, leading to a folded conformation of the tetradentate ligand in the methanol derivative **C2′** (Figure 1, Figure S3, Supporting Information).

In order to determine whether the coordination environment of Co^{II} in the molecular structure also persists in solution, UV/Vis/NIR spectra for **C1**, **C2** and **C2′** were recorded for both solid and in solution (Figure 2). In general, for all complexes the absorption band structure of the spectra in solution is comparable with those obtained from the solid complexes with only minor shifts of the absorption bands. Likewise, spectra of **C1** and **C2** reveal each two absorption maxima at 462 nm and 1012 nm for **C1** as well as 486 and 926 nm for **C2**, respectively, which is in line with a comparable molecular structure for these complexes. Likewise, complex **C2′** showed a broad absorption band at 1030 nm and at 500 nm comparable with those of the other Co^{II} complexes supporting the octahedral coordination in solution. The more complex band structure at around 500 nm for **C2′** compared with those of **C1** and **C2** is suggested to be a result of the altered coordination environment and ligand conformation in **C2′**. For both Co complexes of **L1** and **L4**, the magnetic moment was determined by the Evans method to allow for conclusions about the spin state of the metal center. For **C1** in acetonitrile, a magnetic moment of μ_{eff} = 2.36 μ_B was determined, which indicates a spin S = 1/2 system. Thus, **C1** features a low spin Co^{II} center in accordance with previous reports on this complex.[39] For the Co^{II} complex comprising **L4**, however, a significantly higher magnetic moment of μ_{eff} = 3.78 μ_B (**C2**) or μ_{eff} = 4.16 μ_B (**C2′**), respectively, was observed. In accordance with literature reports on Co^{II} complexes, these values can be best explained with a high spin Co^{II} compound.[41] Consequently, introduction of sulfur as donor atom into the ligand system has a direct influence on the spin state of the metal center.

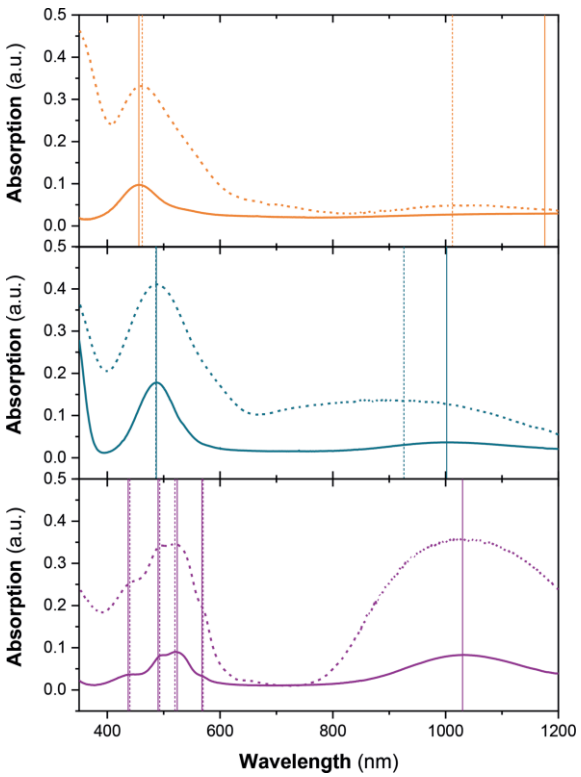

Figure 2. UV/Vis/NIR spectra of Co^{II} complexes **C1** (top), **C2** (middle) and **C2′** (bottom) in acetonitrile solutions (solid lines) and as solid sample (dashed lines).

Cyclic Voltammetry

The Co complexes **C1** and **C2** were subsequently characterized by cyclic voltammetry (CV) in dry acetonitrile with 0.1 M $[(n\text{Bu})_4\text{N})](PF_6)$ as supporting electrolyte in an argon atmosphere (Figure 3). The CV of **C1** reveals a quasi-reversible redox process at $E_{1/2}$ = 0.09 V vs. Fc/Fc^+ for the $Co^{III/II}$ couple and two distinct one electron reduction waves at –1.98 and –2.21 V vs. Fc/Fc^+ for irreversible $Co^{II} \rightarrow Co^{I}$ and $Co^{I} \rightarrow Co^{0}$ reduction, which is in line with previously reported electrochemical data for $[Co^{III}(\mathbf{L1})(Cl)](Cl)_2$.[33] Contrary, replacement of the two nitrogen atoms by sulfur within the ligand scaffold leads to a facilitated reduction of $Co^{II} \rightarrow Co^{I}$ at –1.5 V vs. Fc/Fc^+ and $Co^{I} \rightarrow Co^{0}$ at –1.92 V vs. Fc/Fc^+ for **C2** (Figure 3). Additionally, the reversible $Co^{III/II}$ couple is shifted 150 mV to more positive potential. While for **C1** both reductive signals in the cathodic region are irreversible, for **C2**

the reduction of $Co^{II} \rightarrow Co^{I}$ becomes reversible when the CV scan is reversed at –1.7 V vs. Fc/Fc^+ displaying a $E_{1/2}$ of –1.5 V vs. Fc/Fc^+ (Figure 3, dashed line).

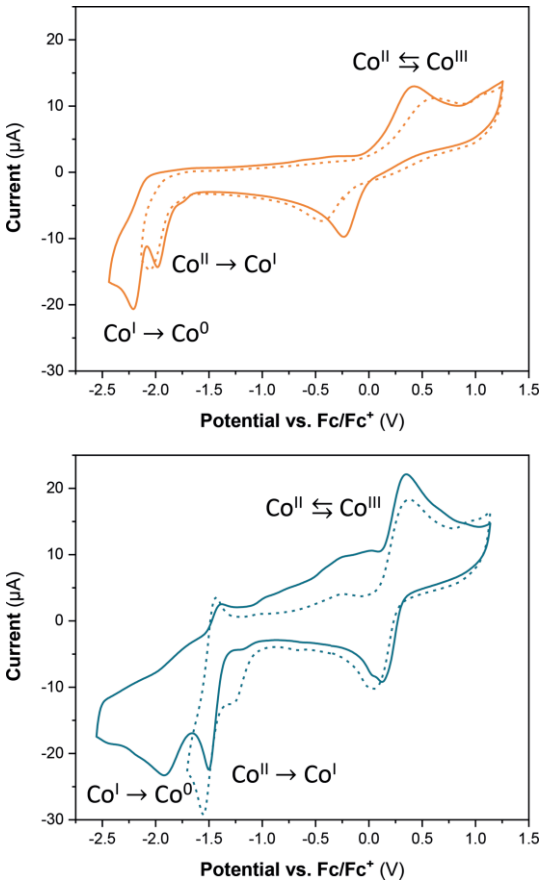

Figure 3. Cyclic voltammograms with various turning points of 1 mM **C1** (top) and **C2** (bottom) in acetonitrile with 0.1 M $[(n\text{Bu})_4\text{N}](PF_6)$ at 100 $mV \cdot s^{-1}$.

Compared to the electrochemical measurements in pure acetonitrile, **C2** showed a completely different behavior in acetonitrile/water mixtures (4 : 1) (Figure 4). Herein, the CV still reveals two reductive waves. The signal previously assigned to the $Co^{II} \rightarrow Co^{I}$ reduction, however, is shifted to a slightly more negative potential of –1.57 V vs. Fc/Fc^+, whereas the $Co^{I} \rightarrow Co^{0}$ reduction is shifted 180 mV more positive to –1.7 V vs. Fc/Fc^+ with a permanently irreversible $Co^{II} \rightarrow Co^{I}$ couple. The slightly increased current at such negative values further indicates the beginning of catalytic processes – most likely water reduction to afford hydrogen. In comparison, the CV of **C1** in acetonitrile/water mixture, within the potential window is completely featureless, except of the strong catalytic current presumably due to hydrogen formation (Figure 4).

Since the Co^{II} complexes are known to act as catalysts for the reduction of CO_2, electrochemical studies in acetonitrile/water mixtures of **C1** and **C2** were also performed in the presence of CO_2. For this purpose, prior to the measurements the electrolyte containing the corresponding Co complex was saturated with CO_2 by purging the gas through the solution. In case of **C1**, no significant change of the CV was obtained in comparison to the measurement without CO_2. CVs of **C2**, recorded in the presence of CO_2, however, revealed a clearly altered shape. In addition to a slight anodic shift of the irreversible Co-centered reduction wave, an increased catalytic current occurs upon the CO_2 purge. This behavior indicates that **C2** potentially catalyzes the hydrogen formation and CO_2 reduction. Since this current increase is already observed at the first reductive signal at –1.54 V vs. Fc/Fc^+, it seems that the Co^{I} intermediate acts as the catalytically active species.

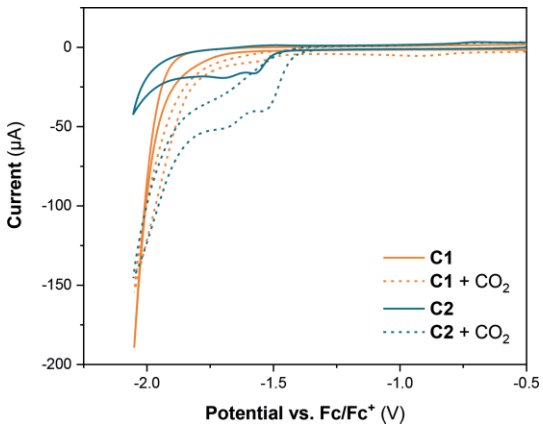

Figure 4. Cyclic voltammograms of 1 mM **C1** (orange) and **C2** (blue) in acetonitrile/water (4:1) under argon (solid lines) and saturated with CO_2 (dashed lines) with 0.1 M $[(n\text{Bu})_4\text{N}](PF_6)$ at 100 $mV \cdot s^{-1}$.

CO_2 Reduction

In order to proof the nature of the formed products, controlled potential coulometry was exemplarily performed with **C2** in the presence of CO_2 for 23 h at –1.92 V vs. Fc/Fc^+. The long-term measurement was performed in a one-compartment cell using a three-electrode set-up with a glassy carbon working electrode, Ag wire as pseudo-reference and Pt wire as counter electrode. After saturation of the electrolyte with CO_2, the cell was sealed for the time of the experiment. Within the first 7 h, quantitative analyses of the headspace via GC-MS were performed for the gaseous products in regular intervals (Figure 5). After 23 h, the electrolyte was likewise examined for additional soluble reduction products. While after one hour electrolysis only CO was detected in low amounts, H_2 occurred from the competing proton reduction with increasing amounts with ongoing reaction time. While after 3 h, a CO : H_2 ratio of 3 : 1 was detected, this ratio decreased to 1.6 : 1 after 7 h. After 23 h electrolysis, proton reduction clearly dominates over CO_2 reduction leading to a product ratio of 0.3 : 1 in favor of H_2. In addition, as a result of acetonitrile decomposition, ethylene (165 ppm) and ethane (566 ppm) were observed in the headspace of the reaction mixture and acetaldehyde (106 $g \cdot mL^{-1}$) as well as ethanol (28 $g \cdot mol^{-1}$) were identified within the aqueous phase. Additionally, it should also be mentioned that during the long-term measurements, the homogeneous catalyst **C2** was deposited on the glassy carbon electrode, visible by the formation of a solid on the electrode as well as a decolorization of the electrolyte solution. In total, after 23 h long-term electrolysis a total faradaic efficiency of 42.4 % was achieved

ignoring any potential electron transfer processes to the Co complex and subsequent decomposition pathways itself. Notably, these results reveal a comparable electrochemical behavior of **C2** as was reported earlier for **C1**.[25,31]

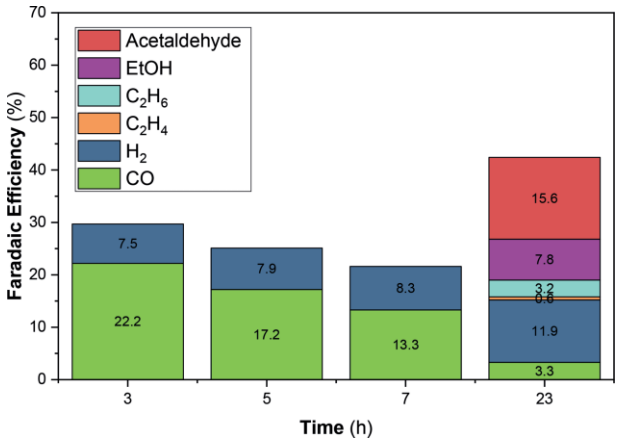

Figure 5. Faradaic efficiencies (FE) for long-term electrolysis at –1.92 V vs. Fc/Fc^+ of CO_2 saturated acetonitrile/water (4:1) mixtures in presence of **C2** as catalysts with $[(n\text{Bu}_4)\text{N}](PF_6)$ for 23 h. Note that the formation of acetaldehyde, ethanol, C_2H_6 and C_2H_4 stems from a degradation of acetonitrile catalyzed by **C2**.

Proton Reduction

As shown by long-term electrolysis of **C2** in CO_2 saturated acetonitrile/water mixtures (4 : 1), the CO_2 reduction was suppressed by proton reduction. This competing process leads to a shift of the CO : H_2 ratio in favor of the hydrogen evolution. This observation pointed our attention to the hydrogen evolution reaction (HER) using **C1** and **C2**. Thus, titration experiments in acetonitrile were performed for **C1** and **C2** (1 mM) in the presence of varying amounts of acetic acid. Addition of each equivalent acetic acid caused for both **C1** and **C2** a continuous increase in the current of both reduction waves (Figure 6). Since the current increase is already observed for the $Co^{II/I}$ couple, it can be assumed that a Co^I intermediate is responsible for the behavior observed. Furthermore, the anodic potential shift of this reduction wave upon increasing the equimolar amount of acidic acid suggests protonation of this Co^I state. In the presence of an excess of acetic acid (0.1 M), proton reduction using **C1** is facilitated at overpotential of –1.53 V vs. Fc/Fc^+ at 0.1 mA (Figure S4, Supporting Information).

In comparison, **C2** enables HER at –1.57 V vs. Fc/Fc^+ at –0.1 mA, 40 mV more negative potential, under otherwise identical conditions. Notably, H_2 evolution in absence of any Co^{II} catalyst takes place only at –1.98 V vs. Fc/Fc^+ at –0.1 mA suggesting that the **C1** and **C2** are catalysts for the H_2 formation (Figure S4). Controlled potential coulometry experiments were subsequently preformed in acetonitrile containing 0.1 M acetic acid. The potential was set to –1.83 V vs. Fc/Fc^+ for **C1** as well as for **C2** for 5 h and hydrogen amount quantified hourly via online GC. While with **C2** a constant faradaic efficiency of about 50 % was observed, the faradaic efficiency of complex **C1** increased continuously from about 64 to 72 %

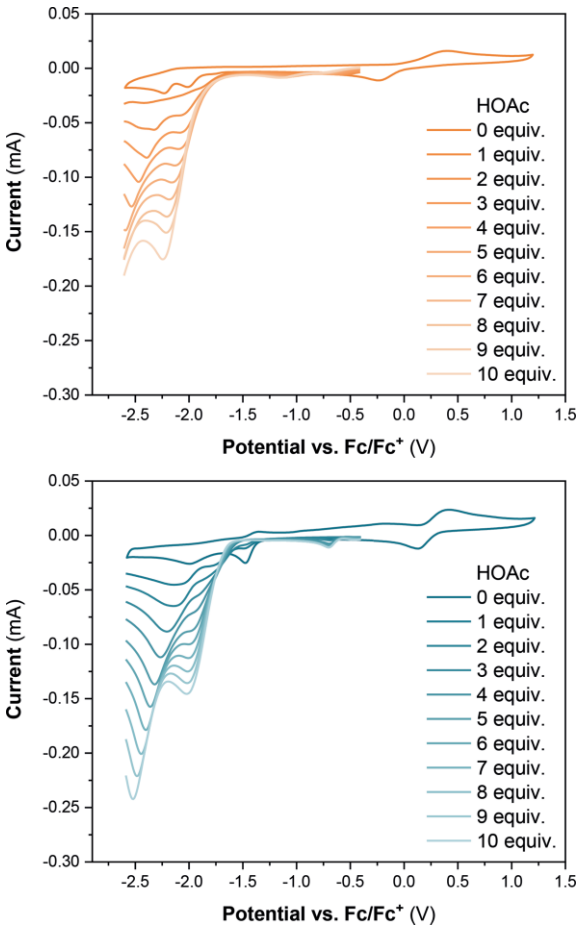

Figure 6. Cyclic voltammograms of 1 mM **C1** (top) and **C2** (bottom) with increasing equivalents of acetic acid (HOAc) in acetonitrile containing 0.1 M $[(n\text{Bu})_4\text{N}](PF_6)$ at 100 $mV \cdot s^{-1}$.

within five hours (Figure 7). Notably, the low faradaic efficiencies observed suggest that side reactions take place that do not result in the formation of H_2 and are not accommodated in the displayed faradaic efficiency. However, the obtained data suggests that **C1** is more efficient in catalyzing the HER at identical potentials than **C2**. Thus, the exchange of nitrogen to sulfur within the cyclam-based ligand scaffold leads to a hampered proton reduction under acidic conditions.

This behavior indicates that the secondary amines are an essential structural feature for the HER. Mechanistic studies on Co-based HER catalysts revealed that the reduction to afford the catalytically active Co^I or Co^0 species followed by protonation to produce a metal-hydride, Co^{III}–H or Co^{II}-H, are key steps within the catalysis.[12]

Conclusions

In summary, we herein describe the synthesis and characterization of hitherto unprecedented S containing cobalt complex **C2** along with its performance in the electrocatalytic reduction of protons and CO_2 in comparison to the literature known cobalt complex **C1**. Notably, the incorporation of sulfur leads to a high spin state in **C2** rather than the observed low spin state

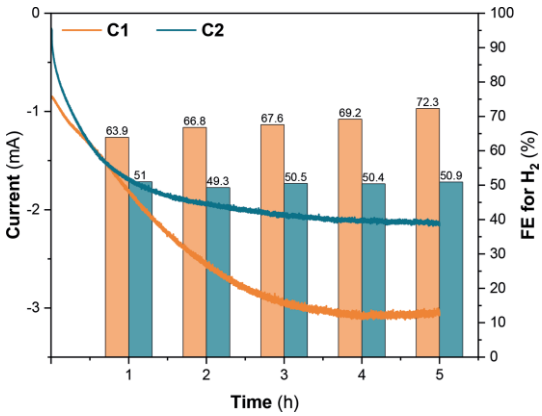

Figure 7. Controlled potential coulometry experiments without catalyst (blank) and with catalyst **C1** (orange) and **C2** (blue) in presence of 0.1 M acetic acid in acetonitrile containing 0.1 M $[(n\text{Bu})_4\text{N}](\text{PF}_6)$ and corresponding faradaic efficiencies for H_2 for both complexes.

of **C1**. The altered electronics lead to a facilitated ligand exchange in **C2** visible by pronounced solvent exchange of methanol vs. acetonitrile. While both complexes **C1** and **C2** allow for the CO_2 reduction to afford CO at –1.92 V vs. Fc/Fc^+. However, H_2 formation is generally favored and thus complexes **C1** and **C2** likewise enable the conversion of protons to H_2. However, in contrast to $[Co(cyclam)]^{2+}$, $[Co(dithiacyclam)]^{2+}$ complexes are more prone to deposition/decomposition on the working electrode. Thus, an overall lowered efficiency for $[Co(dithiacyclam)]^{2+}$ for the electrocatalytic processes is observed in comparison to the $[Co(cyclam)]^{2+}$ congener.

Experimental Section

All reactions were performed in a dry Ar or N_2 atmosphere using standard Schlenk techniques or by working in a glovebox. Starting materials and chemicals were obtained from commercial suppliers and used without further purification. Prior to their use, all solvents were dried and degassed according to standard methods. 1,8-Dithiacyclam-4,11-diazacyclotetradecane (dithiacyclam) **L4** was synthesized according to literature-known procedures.[42] Mass spectra were obtained with a Bruker Daltonics Esquire 6000 instrument. IR spectra were recorded on a Bruker Tensor 27 FT-IR attached with a Pike Miracle ATR unit and are reported in cm^{-1}. UV/Vis/NIR spectra were recorded with a Jasco V-670 at 25 °C. **Caution!** Perchlorate salts of metal complex with organic ligands are potentially explosive. They should be handled with care and prepared only in small quantities.

$[Co(L1)(CH_3CN)_2](ClO_4)_2$ (C1): Compound **L1** (250 mg, 1.25 mmol) was dissolved in 3 mL acetonitrile and a solution of $Co(ClO_4)_2{\cdot}6H_2O$ (456 mg, 1.25 mmol) in 5 mL acetonitrile was added dropwise. After the addition was completed, the reaction mixture was stirred for 2 d at room temperature concomitant with a color change to orange. Subsequently, the reaction mixture was filtered and reduced to half of its original volume. Co complex **C1** was then precipitated as an orange solid by addition of diethyl ether. The formed solid was filtered off and washed with cold diethyl ether as well as hexane. After drying under vacuum, compound **C1** was afforded as an orange solid in 75 % (506 mg, 0.94 mmol) yield. Crystals could be obtained by slow diffusion of diethyl ether into a concentrated acetonitrile solution of **C1**. **ESI-MS**: calcd. for $[C_{10}H_{24}CoN_4{+}H]^+$: m/z = 260.1, and $[C_{10}H_{24}CoN_4{+}ClO_4]^+$: m/z = 358.1; found: 258.1 and 357.9. $C_{12}H_{27}Cl_2CoN_5O_8$: calcd. C, 28.87; H, 5.45; N, 14.20 %; found: C, 28.96; H, 5.01; N, 14.55 %. **IR** (ATR) $\tilde{\nu}$ = 3244, 2939, 2885, 2297, 2263, 1630, 1455, 1437, 1078, 1011, 931 cm^{-1}. **UV/Vis/NIR** (CH_3CN, nm): 456, 1176.

$[Co(L4)(CH_3CN)_2](ClO_4)_2$ (C2): Compound **L4** (250 mg, 1.06 mmol) was suspended in 5 mL acetonitrile and a solution of $Co(ClO_4)_2{\cdot}6H_2O$ (390 mg, 1.06 mmol) in 5 mL acetonitrile was added dropwise. After the addition was completed, the reaction mixture was stirred for 2 days at room temperature. Within this time a pale pink precipitate was formed. The precipitate was then filtered off and washed with cold diethyl ether and hexane. After drying under vacuum, the pink solid was recrystallized from an acetonitrile solution layered with diethyl ether affording compound **C2** (L = CH_3CN) as a pale rose solid in 85 % (520 mg, 0.9 mmol) yield. Single crystals could be obtained by slow diffusion of diethyl ether into a concentrated acetonitrile solution of **C2**. **ESI-MS**: calcd. for $[C_{10}H_{22}CoN_2S_2{+}H]^+$: 292.1, and $[C_{10}H_{22}CoN_2S_2{+}ClO_4]^+$: 392.0; found: 292.0 and 391.9. $C_{14}H_{28}Cl_2CoN_4O_8S_2$: calcd. C, 29.28; H, 4.91; N, 9.76 %; found: C, 28.89; H, 5.11; N, 9.78 %. **IR** (ATR) $\tilde{\nu}$ = 3218, 2968, 2936, 2295, 2260, 1461, 1424, 1303, 1232, 1183, 1090, 982 cm^{-1}. **UV/Vis/NIR** (CH_3CN, nm): 487, 1002.

$[Co(L4)(CH_3OH)_2](ClO_4)_2$ (C2′): Complex **C2** was dissolved in methanol and stirred for 30 min at room temperature. Removing the solvent and repeating this procedure two times afforded **C2'** as a rose solid. Single crystals could be obtained by slow diffusion of diethyl ether into a concentrated methanol solution of **C2′**. **ESI-MS**: calcd. for $[C_{10}H_{22}CoN_2S_2{+}H]^+$: 292.1, and $[C_{10}H_{22}CoN_2S_2{+}ClO_4]^+$: 392.0; found: 292.0 and 391.9. $C_{12}H_{30}Cl_2CoN_2O_{10}S_2$: calcd. C, 25.91; H, 5.44; N, 5.04 %; found: C, 25.50; H, 5.46; N, 5.13 %. **IR** (ATR) $\tilde{\nu}$ = 3384, 3259, 2950, 2883, 1638, 1424, 1308, 1234, 1089, 1056, 999, 623 cm^{-1}. **UV/Vis/NIR** (CH_3OH, nm): 437, 490, 524, 566, 1030.

Electrochemistry: Electrochemical studies were performed using a PalmSens3 or PalmSens4 potentiostat in a standard three-electrode set-up. As working electrode (WE) a glassy carbon electrode, as counter electrode (CE) a Pt wire and as pseudo-reference electrode (RE) an Ag wire was used. Prior to its use, the working electrode was successively polished and subsequently sonicated in deionized acetonitrile. Tetrabutylammonium hexafluorophosphate $[(n\text{Bu})_4\text{N}](\text{PF}_6)$ 0.1 M was used as conducting salt in all electrochemical measurements either in anhydrous acetonitrile or a mixture of acetonitrile/water (4:1). The electrochemical experiments were performed under dry Ar atmosphere in a glovebox. All cyclic voltammograms were recorded at a scan rate of 100 $mV{\cdot}s^{-1}$ and all pseudo-referenced potentials were referenced against the ferrocene/ferrocenium couple ($E_{1/2}$ = 0.4 V vs. NHE).

Controlled potential coulometry for CO_2 reduction was performed in a one-compartment cell in a glovebox using a standard three electrode set-up with glassy carbon working electrode (WE), Pt wire as counter (CE) and Ag wire as pseudo-reference electrode (RE). Acetonitrile/water (4:1) mixture with 0.1 M $[(n\text{Bu})_4\text{N}](\text{PF}_6)$ as electrolyte was saturated with CO_2 prior the long-term experiment. Headspace gas composition and liquid phase composition were performed using a Shimadzu GCMS-QP2020 system equipped with two capillary columns and a MS detector. Gas separation was performed via hand injection using a Carboxen 1010 PLOT fused silica capillary GC column (L × I.D. 30 m × 0.32 mm, average thickness 15 µm) and liquid phase separation was performed via headspace analysis using a SH-Rtx-200ms fused silica capillary GC column (L × I.D. 30 m × 0.25 mm, average thickness 1 µm). Helium was used as carrier gas. The following gaseous

and liquid products/components were assayed via the GCMS system: H_2, O_2, N_2, CO, CH_4, C_2H_4, C_2H_6, methanol, ethanol, propanol, formate/formic acid, acetate/acetic acid, propionate/propionic acid, acetaldehyde and propionaldehyde. Liquid samples were acidified with concentrated sulfuric acid (10 : 1) before injection.

Controlled potential coulometry for HER was performed in a H-type two-compartment cell under inert atmosphere separating anodic and cathodic space by a Nafion membrane. A standard three-electrode setup was used with glassy carbon working electrode (WE), Pt mesh as counter (CE) and Ag wire as pseudo-reference electrode (RE). As solvent acetonitrile with 0.1 M $[(n\text{Bu})_4\text{N}](\text{PF}_6)$ as electrolyte and acetic acid 0.1 M was used. CPC was performed at defined potential and afterwards referenced against the ferrocene/ferrocenium couple. Hydrogen production was quantified in an online set-up using an Agilent Technologies 7820A gas chromatograph equipped with a thermal conductivity detector (TCD) and a flame ionization detector (FID) as well as a methanizer. Gas separation was performed using a two-column separation system (HP-PLOT Q 3 m × 0.53 mm × 40 µm column and HP-Molesieves 5 Å 30 m × 0.53 mm × 25 µm) using argon as carrier gas.

X-ray Data Collection and Structure Solution Refinement: Single crystals suitable for X-ray diffraction experiments were analyzed either using a Rigaku Oxford diffraction XtaLAB SuperNova equipped with an Atlas CCD detector or a Rigaku Oxford diffraction XtaLAB Synergy-S with an HyPix-6000HE detector (Cu-K_α, λ = 1.54184 Å for both diffractometers). The crystals were handled in perfluorinated oil, mounted onto fiber loops and cooled by a flow of cold nitrogen (Oxford Cryostream) throughout the experiments. The obtained diffraction data was analyzed using the CrysAlis^{Pro} software package. Structure solutions were computed using the programs ShelXS[43] (direct methods) or ShelXT[44] (intrinsic phasing) and were refined against F^2 using ShelXL.[45] Hydrogen atoms were added in calculated positions. The program package OLEX^2 [46] served as graphical interface.

Supporting Information (see footnote on the first page of this article): Supporting information contains IR spectra, molecular structures, linear sweep voltammograms as well as crystal data and structure refinements.

Acknowledgements

This work was supported by the Fonds of the Chemical Industry (Liebig Grant) to U.-P. A. and the Deutsche Forschungsgemeinschaft (Emmy Noether Grant) to U.-P. A. This work was supported by the Fraunhofer Internal Programs (Attract, Grant No. 097–602175) as well as the Fraunhofer Cluster of Excellence CINES. The work was funded by the Deutsche Forschungsgemeinschaft (DFG, German Research Foundation) under Germany's Excellence Strategy, EXC-2033 (Projektnr. 390677874). Open access funding enabled and organized by Projekt DEAL.

Keywords: Dithiacyclam; Cobalt; Electrocatalysis; Carbon dioxide; Hydrogen

References

[1] E. E. Benson, C. P. Kubiak, A. J. Sathrum, J. M. Smieja, *Chem. Soc. Rev.* **2009**, *38*, 89–99.
[2] M. Aresta, Ed., *Carbon Dioxide as Chemical Feedstock*, Wiley-VCH, Weinheim, **2010**.
[3] A. M. Appel, J. E. Bercaw, A. B. Bocarsly, H. Dobbek, D. L. DuBois, M. Dupuis, J. G. Ferry, E. Fujita, R. Hille, P. J. A. Kenis, et al., *Chem. Rev.* **2013**, *113*, 6621–6658.
[4] N. Dubouis, A. Grimaud, *Chem. Sci.* **2019**, *10*, 9165–9181.
[5] Z. Thammavongsy, I. P. Mercer, J. Y. Yang, *Chem. Commun.* **2019**, *55*, 10342–10358.
[6] L. Schlapbach, A. Züttel, *Nature* **2001**, *414*, 353–358.
[7] M. M. May, H.-J. Lewerenz, D. Lackner, F. Dimroth, T. Hannappel, *Nat. Commun.* **2015**, *6*, 8286.
[8] B. P. Sullivan, K. Krist, H. E. Guard, Eds., *Electrochemical and Electrocatalytic Reactions of Carbon Dioxide*, Elsevier, Amsterdam; New York, **1993**.
[9] M. Wang, L. Chen, L. Sun, *Energy Environ. Sci.* **2012**, *5*, 6763.
[10] J. Qiao, Y. Liu, F. Hong, J. Zhang, *Chem. Soc. Rev.* **2014**, *43*, 631–675.
[11] R. Francke, B. Schille, M. Roemelt, *Chem. Rev.* **2018**, *118*, 4631–4701.
[12] K. E. Dalle, J. Warnan, J. J. Leung, B. Reuillard, I. S. Karmel, E. Reisner, *Chem. Rev.* **2019**, *119*, 2752–2875.
[13] W. Lubitz, H. Ogata, O. Rüdiger, E. Reijerse, *Chem. Rev.* **2014**, *114*, 4081–4148.
[14] J. Esselborn, N. Muraki, K. Klein, V. Engelbrecht, N. Metzler-Nolte, U.-P. Apfel, E. Hofmann, G. Kurisu, T. Happe, *Chem. Sci.* **2016**, *7*, 959–968.
[15] H. Dobbek, *Science* **2001**, *293*, 1281–1285.
[16] H. Dobbek, L. Gremer, R. Kiefersauer, R. Huber, O. Meyer, *Proc. Natl. Acad. Sci.* **2002**, *99*, 15971–15976.
[17] J.-H. Jeoung, H. Dobbek, *Science* **2007**, *318*, 1461–1464.
[18] K. Hiratsuka, K. Takahashi, H. Sasaki, S. Toshima, *Chem. Lett.* **1977**, *6*, 1137–1140.
[19] O. Enoki, T. Imaoka, K. Yamamoto, *Macromol. Symp.* **2003**, *204*, 151–158.
[20] G. F. Manbeck, E. Fujita, *J. Porphyrins Phthalocyanines* **2015**, *19*, 45–64.
[21] M. Razavet, V. Artero, M. Fontecave, *Inorg. Chem.* **2005**, *44*, 4786–4795.
[22] W. T. Eckenhoff, W. R. McNamara, P. Du, R. Eisenberg, *Biochim. Biophys. Acta, Bioenergetics* **2013**, *1827*, 958–973.
[23] W. T. Eckenhoff, *Coord. Chem. Rev.* **2018**, *373*, 295–316.
[24] K. C. Cartwright, A. M. Davies, J. A. Tunge, *Eur. J. Org. Chem.* **2019**, DOI 10.1002/ejoc.201901170.
[25] B. J. Fisher, R. Eisenberg, *J. Am. Chem. Soc.* **1980**, *102*, 7361–7363.
[26] M. Beley, J. P. Collin, R. Ruppert, J. P. Sauvage, *J. Am. Chem. Soc.* **1986**, *108*, 7461–7467.
[27] J. Collin, J. P. Sauvage, *Coord. Chem. Rev.* **1989**, *93*, 245–268.
[28] G. B. Balazs, F. C. Anson, *J. Electroanal. Chem.* **1992**, *322*, 325–345.
[29] J. D. Froehlich, C. P. Kubiak, *Inorg. Chem.* **2012**, *51*, 3932–3934.
[30] J. D. Froehlich, C. P. Kubiak, *J. Am. Chem. Soc.* **2015**, *137*, 3565–3573.
[31] A. H. A. Tinnemans, T. P. M. Koster, D. H. M. W. Thewissen, A. Mackor, *Recl. Trav. Chim. Pays-Bas* **2010**, *103*, 288–295.
[32] S. Matsuoka, K. Yamamoto, C. Pac, S. Yanagida, *Chem. Lett.* **1991**, *20*, 2099–2100.
[33] S. Matsuoka, K. Yamamoto, T. Ogata, M. Kusaba, N. Nakashima, E. Fujita, S. Yanagida, *J. Am. Chem. Soc.* **1993**, *115*, 601–609.
[34] T. Ogata, S. Yanagida, B. S. Brunschwig, E. Fujita, *J. Am. Chem. Soc.* **1995**, *117*, 6708–6716.
[35] S. Yanagida, T. Ogata, Y. Yamamoto, Y. Wada, K. Murakoshi, M. Kusaba, N. Nakashima, A. Ishida, S. Takamuku, *Energy Convers. Management* **1995**, *36*, 601–604.
[36] T. Ogata, Y. Yamamoto, Y. Wada, K. Murakoshi, M. Kusaba, N. Nakashima, A. Ishida, S. Takamuku, S. Yanagida, *J. Phys. Chem.* **1995**, *99*, 11916–11922.
[37] J. Honores, D. Quezada, M. García, K. Calfumán, J. P. Muena, M. J. Aguirre, M. C. Arévalo, M. Isaacs, *Green Chem.* **2017**, *19*, 1155–1162.

[38] P. Gerschel, K. Warm, E. R. Farquhar, U. Englert, M. L. Reback, D. Siegmund, K. Ray, U.-P. Apfel, *Dalton Trans.* **2019**, DOI 10.1039/C8DT04740E.
[39] J. F. Endicott, J. Lilie, J. M. Kuszaj, B. S. Ramaswamy, W. G. Schmonsees, M. G. Simic, M. D. Glick, D. P. Rillema, *J. Am. Chem. Soc.* **1977**, *99*, 429–439.
[40] T. Yokoyama, H. Kitagawa, H. Iwasawa, M. Zenki, *Inorg. Chim. Acta* **1996**, *253*, 1–6.
[41] E. K. Barefield, D. H. Busch, S. M. Nelson, *Q. Rev. Chem. Soc.* **1968**, *22*, 457.
[42] T. L. Walker, W. Malasi, S. Bhide, T. Parker, D. Zhang, A. Freedman, J. M. Modarelli, J. T. Engle, C. J. Ziegler, P. Custer, et al., *Tetrahedron Lett.* **2012**, *53*, 6548–6551.
[43] G. M. Sheldrick, *Acta Crystallogr., Sect. A, Found. Crystallogr.* **2008**, *64*, 112–122.
[44] G. M. Sheldrick, *Acta Crystallogr., Sect. A, Found. Adv.* **2015**, *71*, 3–8.
[45] G. M. Sheldrick, *Acta Crystallogr., Sect. C, Struct. Chem.* **2015**, *71*, 3–8.
[46] O. V. Dolomanov, L. J. Bourhis, R. J. Gildea, J. A. K. Howard, H. Puschmann, *J. Appl. Crystallogr.* **2009**, *42*, 339–341.

Received: December 23, 2019
Published Online: February 28, 2020

